ACS Catalysis

Research Article

pubs.acs.org/acscatalysis

Crystal Growth Kinetics as a Tool for Controlling the Catalytic Performance of a FAU-Type Basic Catalyst

Satoshi Inagaki,[†] Karine Thomas,[‡] Valérie Ruaux,[‡] Guillaume Clet,[‡] Toru Wakihara,[§] Shoma Shinoda,[†] Sae Okamura,[†] Yoshihiro Kubota,[†] and Valentin Valtchev*[,‡]

[†]Division of Materials Science and Chemical Engineering, Yokohama National University, 79-5 Tokiwadai, Hodogaya-ku, Yokohama 240-8501, Japan

[‡]Laboratoire Catalyse et Spectrochimie, ENSICAEN, Université de Caen, CNRS, 6 Boulevard du Maréchal Juin, 14050 Caen, France

[§]Department of Chemical System Engineering, School of Engineering, The University of Tokyo, 7-3-1 Hongo, Bunkyo-ku, Tokyo 113-8656, Japan

Supporting Information

ABSTRACT: This study reports on the catalytic performance of nanosized zeolite X crystals and their precursors in the reaction of benzaldehyde with ethyl cyanoacetate. Crystal growth kinetics of FAU-type zeolite is studied at low temperature (35 °C) in order to discriminate different crystallization stages. First X-ray crystalline material is detected after 6 days of hydrothermal treatment. The formation of the crystalline phase is preceded by changes in the ring structure of an aluminosilicate precursor as revealed by the combined Raman−HEXRD−solid-state NMR analyses. The set of experimental data shows that these changes are related to the reorganization of the gel structure and the formation of zeolite units. Prior to the appearance of crystalline material, the apparently amorphous solid exhibits chemical composition and short-range order organization similar to that of a crystalline FAU-type zeolite. Knoevenagel condensation was used to test the catalytic activity of a series of zeolite intermediates and nanosized zeolite crystals. The amorphous precursor obtained after 5 days of hydrothermal treatment showed the highest yield of ethyl α-cyanocinnamate. Superior catalytic performance of this material was attributed to the combination of strong basic sites and less restricted and more accessible structure of the semicrystalline zeolite units. Thus, the crystal growth kinetics of FAU-type zeolite can be used as a tool to tune the properties of a catalyst used in Knoevenagel condensation.

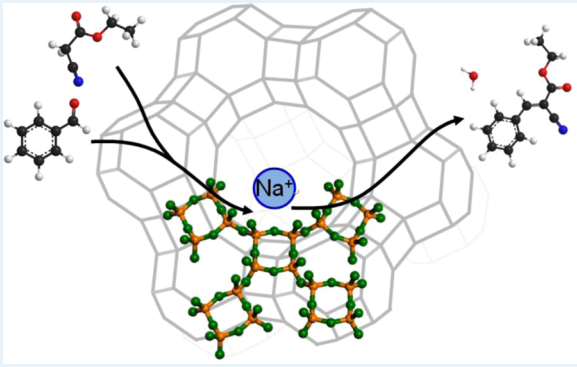

KEYWORDS: *FAU-type zeolite, basic catalysis, active sites accessibility, Knoevenagel condensation, framework basicity*

INTRODUCTION

Zeolites are microporous crystalline aluminosilicates with a negatively charged lattice, due to the isomorphous substitution of Si^{4+} by Al^{3+} in the framework.[1] When the negative charge is neutralized by protons, the zeolites work as a solid catalyst with Brönsted acidity. Alternatively, when alkali or alkali-earth cations neutralize the negative charge of the framework, the zeolite can be considered as solid Lewis acid−base-type materials.[2] Thus, the zeolites impart flexible acid−base properties, which are widely used in heterogeneous catalysis.

Base-catalyzed reactions, including the formation of carbanions as intermediates, are among the technologically most important classes of catalytic conversions in fine-chemical synthesis. Conventional organic reactions often require a stoichiometric amount of liquid base to generate carbanions and produce a stoichiometric amount of metal salts as byproducts. Because homogeneous base-catalyzed reactions present serious drawbacks related to the separation and regeneration of the catalyst, heterogeneous base-catalytic reactions are an attractive alternative as environmentally benign chemical processes.[3−7]

The Knoevenagel condensation, a nucleophilic addition of a carbanion (derived from an active methylene compound) to an electrophilic carbonyl group in the presence of relatively weak base followed by dehydration, is a key step in the commercial production of various bulky pharmaceuticals and has been used as a test reaction for the characterization of solid-base catalysts.[8] Over the past decades, various solid-base catalysts have been applied to this reaction, such as anion-exchange resin,[9] KF,[10] magnesium and aluminum oxides,[11−13] alkali-exchanged and alkali-encapsulated molecular sieves,[14−17] hydrotalcites,[18] amino-group-modified silica materials,[19,20] and clays.[21] Our group has studied organic-modified mesoporous molecular sieves in Knoevenagel[22] and aldol[23] condensation reactions.

Received: April 16, 2014
Revised: June 3, 2014
Published: June 3, 2014

   dx.doi.org/10.1021/cs500153e | ACS Catal. 2014, 4, 2333−2341

The results pointed out that a cooperative effect of the surface silanol and secondary amine may enhance the catalytic activity in the base-catalyzed reactions. More recently, Ogura and co-workers have reported that nitrogen-doped siliceous zeolite[24] and mesoporous silica material[25] were successfully synthesized via NH_3 treatment of siliceous porous materials at high temperatures and that their nitrogen species were as strongly basic as conventional solid-base catalysts for Knoevenagel condensation. Thus, the advances in the preparation of heterogeneous solid-base catalysts are opening the road to environmentally benign chemical processes in fine-chemicals production.

At present 218 zeolite framework types have been approved by the structural commission of the International Zeolite Association.[26] Yet, a few zeotypes have found industrial applications (e.g., the FAU-type zeolites are the most widely used in the field of heterogeneous catalysis and separation processes). This type of zeolite, in particular, its higher silica-containing members zeolite Y and ultrastable Y (USY), are used in refinery fluid catalytic cracking (FCC) processes. FAU-type zeolite, built by stacking layers of sodalite cages ($[4^6 6^8]$) in an ABCABC sequence, possesses 12-ring pore mouths (0.74 nm × 0.74 nm) that are three-dimensionally connected with internal supercages (ca. 1.3 nm in diameter). Different alkali cation (Li^+, Na^+, K^+, Cs^+) forms of FAU-type zeolite have been studied as solid-base catalyst in the Knoevenagel condensation reaction without employing a solvent.[14] Among different cation-exchanged forms, the Cs^+ form of low-silica FAU-type material (zeolite X) showed the highest catalytic activity due to the decrease in the average electronegativity of the zeolite framework. On the other hand, the FAU-type zeolite containing methyl-substituted ammonium cations are much more basic than those containing Cs^+.[27] However, only conventional micrometer-sized crystals were used up to now. Nanosized zeolites offer certain advantages in catalytic processes, especially when bulky molecules have to be processed. Shorter diffusion paths, large external surface areas, and high surface activity of nanozeolites are expected to have a great impact on the performance of zeolite-type solid-base catalysts.[28]

Zeolites are metastable phases formed under hydrothermal conditions. In nature, alkali (alkali earth) cation−water complexes play the role of structure directing agents that conduct the formation of an aluminosilicate framework. In laboratory conditions, organic structure-directing agents (SDA) are often used instead of/in addition to alkali cations. For instance, the tetramethylammonium (Me_4N^+) cation has been used as a structure-directing agent for the synthesis of FAU-type nanoparticles.[29−33] Although the use of organic SDAs allows better control of zeolite characteristics such as crystal sizes and crystal size distributions, their large scale application is not appreciated. From a practical point of view, the hydrothermal synthesis of zeolite nanocrystals without organic SDAs is highly desirable from environmental and economical considerations. Hence, the synthesis of FAU-type nanocrystals from organic template-free systems have been the objective of a number of studies.[34−39]

Among different factors controlling zeolite formation the aluminosilicate-ring structures in zeolite precursor systems is a key issue that needs to be highlighted if the goal is rational design of zeolite properties. For instance, the FAU-type unit cell, consisting of 192 T atoms (2.43 nm × 2.43 nm × 2.43 nm) comprises the periodic arrangement of different building units such as four- (4R) and six- (6R) member rings. Different physical and chemical methods have been used to study the zeolite formation. Raman spectroscopy is one of the most useful techniques to identify the structures of aluminosilicate rings and thus to provide molecular information on the zeolite precursors.[40−42] On the basis of Raman spectroscopic studies, Dutta et al.[43,44] and Li et al.[45−47] have proposed a model of FAU-type zeolite formation. According to this model, the 4MRs formed in the initial gel interconnect each other via 6MRs to form the FAU-type framework.

Lately high-energy X-ray diffraction (HEXRD) is widely used to analyze the medium-range structure of zeolitic precursors[48−52] and distorted zeolite materials[53,54] that provide important information on zeolite crystal formation. These studies revealed that a medium-range order occurred in the amorphous phase prior to the formation of zeolite framework. Important advances in the understanding of zeolite formation were achieved by the analysis of chemical and physical changes in sodium-rich aluminosilicate gels yielding FAU-,[35,36] LTA-[55−57] and EMT-type[58,59] zeolites at ambient temperature. It was found that just before the appearing of the long-range order that can be detected by diffraction methods, the amorphous aluminosilicate precursor already has the composition of the ultimate zeolite material. These findings suggest that at the end of the induction period, the aluminosilicate precursors already possess some of the zeolite characteristics.

The advances in understanding of zeolite formation in organic template free systems were used to prepare highly active solid-base zeolite catalysts. The zeolite crystal growth kinetics was used as a tool to optimize the catalyst preparation in terms of accessibility and activity and tested in Knoevenagel condensation of benzaldehyde with ethyl cyanoacetate.

EXPERIMENTAL SECTION

Sample Preparation. Nanosized FAU-type zeolite was synthesized at 35 °C according to a procedure described in ref 35. The hydrogel was prepared employing sodium hydroxide pellets (97%, Aldrich), sodium aluminate (53% Al_2O_3, 42% Na_2O, Aldrich), sodium silicate solution (10.6% NaOH, 26.5% SiO_2, Aldrich), and distilled water. First, distilled water and NaOH pellets were mixed in a polypropylene bottle and stirred gently until NaOH was completely dissolved. The required amount of sodium aluminate was added and stirred until the solution became transparent, then sodium silicate solution was added dropwise under vigorous stirring. The composition of the resultant hydrogel was $4.32Na_2O/0.2Al_2O_3/1.0SiO_2/200H_2O$. The mixture was stirred gently at room temperature for 90 min and subjected to crystallization in a convection oven at 35 °C from 1 to 14 days. The same initial gel was used to prepare a reference micrometer-sized zeolite X sample at 80 °C for 5 days. After the synthesis, the solid was recovered by suction filtration, washed with distilled water and dried at room temperature overnight. A part of the initial gel obtained after 90 min stirring was also recovered according to the above procedure and used as a reference.

Characterization. Powder X-ray diffraction (XRD) patterns of the solid products were recorded on a PANalytical X'Pert Pro diffractometer using Cu Kα radiation at 45 kV and 40 mA. The chemical composition of the solids was analyzed by means of inductively coupled plasma using optical emission spectrometer (ICP-OES, Varian). The water contents in the aluminosilicate solids were determined by thermogravimetry (TG, Thermo plus EVO II TG8120, Rigaku) in air in the temperature range of 25−250 °C. Nitrogen adsorption−desorption measurements at −196 °C were carried out by using Autosorb-iQ (Quantachrome Instruments). Before the measurement, the sample was preheated at 120, 150, or 250 °C overnight under evacuation. This series of experiments was performed in order to find the most appropriate conditions that do not lead to irreversible changes in the structure of zeolite precursors.

dx.doi.org/10.1021/cs500153e | ACS Catal. 2014, 4, 2333−2341

Raman spectra of the solids were recorded on a Labram 300 (Horiba Jobin Yvon) instrument. The solids were analyzed by using Nd:YAG green laser (532 nm) and an 1800 lines/mm grating. IR analyses were carried out on a NICOLET 5700 FT-IR spectrometer equipped with a TGS detector. The self-supporting disk (20 mg, 15 mm in diameter) of the sample was placed in an IR cell attached to a conventional close gas-circulation system. The sample disk was pretreated under vacuum at 300 °C for 3 h. After cooling to 25 °C, CO_2 was introduced into the cell, evacuated until 1×10^{-6} mmHg for 15 min, and then the IR spectra were recorded with 128 scans at 4 cm^{-1} of the resolution.

The solid-state magic angle spinning nuclear magnetic resonance (MAS NMR) measurements were performed on an ADVANCEIII-600 (600 MHz (^{1}H), Bruker) with a 4 mm diameter ZrO_2 rotor. The ^{29}Si dipolar-decoupling (DD) MAS NMR spectra (119.2 MHz) were recorded at 30 s of the contact time for 1024 times at 10 kHz. The reference of ^{29}Si chemical shifts was determined with reference to the ^{29}Si signal of hexamethylcyclotrisiloxane at −9.66 ppm. The ^{27}Al direct-excitation (DE) MAS NMR spectra (156.4 MHz) were recorded at 0.5 s of the contact time for 1024 times at a spinning rate of 13.0 kHz. The ^{27}Al chemical shifts were determined using aqueous $Al(NO_3)_3$ solution, the resonance peak of which was adjusted to 0 ppm.

For high-energy X-ray diffraction (HEXRD) analysis, 200 mg of the sample was pressed into a disc, and the measurements were carried out at room temperature. HEXRD spectra were obtained on a horizontal two-axis diffractometer, optimized for structural measurements in glass and liquid and built at the BL04B2 high-energy monochromatic bending magnet beamline of SPring-8. A bent crystal mounted on the monochromator stage fixed at a Bragg angle of 3° in the horizontal plane provides an incident photon energy of 61.63 keV (wavelength: 0.2012 Å) using a bent Si (220) crystal. Pelletized samples were fixed to the sample stage before characterization. Q_{max} collected in this study was 25 $Å^{-1}$. The collected data were subjected to well-established analysis procedures including absorption, background, and Compton scattering corrections followed by normalization to the Faber−Ziman total structure factor, $S(Q)$.[60] The pair distribution function, $G(r)$, is derived from the following equation:

$$G(r) = 4\pi r[\rho(r) - \rho_0] = \frac{2}{\pi}\int_{Q_{min}}^{Q_{max}} \{Q[S(Q) - 1]\sin(Qr)\}dQ$$

where $\rho(r)$ is the microscopic pair density, and ρ_0 is the average number density.

Catalytic Tests. Benzaldehyde (>99%, Merck), ethyl cyanoacetate (>98%, Merck), and dry ethanol (>99.9%, Merck) were used as carbonyl compound, an active methylene compound, and solvent, respectively. The reaction is presented in Scheme 1.

Scheme 1. Knoevenagel Condensation of Benzaldehyde with Ethyl Cyanoacetate

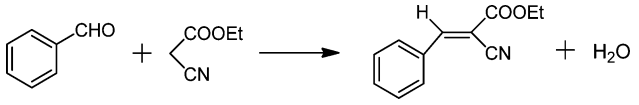

The Knoevenagel condensation was typically carried out in a solution containing 1.0 mmol of benzaldehyde, 1.0 mmol of ethyl cyanoacetate, and 3.0 mL of ethanol. Fifteen milligrams of the solid catalyst without any preliminary pretreatment was added and stirred at 40 or 70 °C for 30 or 60 min, respectively. Gas chromatographic (GC) analysis was performed on a Varian 3900 instrument equipped with a flame ionization detector using a capillary column of Varian VF-1 ms (15 m in length, 0.25 mm in diameter, 0.25 μm in film thickness).

RESULTS AND DISCUSSION

Crystal Growth Kinetics of FAU-Type Zeolite. Figure 1 presents powder X-ray diffraction patterns of the samples obtained after hydrothermal treatment at 35 °C for different periods of time. The solids obtained for up to 5 days are amorphous (Figure 1a−e). After 6 days of synthesis, the first traces of crystalline FAU-type material can be observed (Figure 1f). The crystallinity of the sample obtained after 7 days of synthesis is substantially higher (Figure 1g). The extension of the crystallization time up to 14 days does not change substantially the apparent X-ray crystallinity of the zeolite (Figure 1h−i). It should be noted that the FAU-type samples synthesized at 35 °C show much lower crystallinity with respect to the reference samples obtained at 80 °C for 5 days (Figure 1j). The XRD peaks of low-temperature crystallized materials are broader with lower intensity, which is obviously due to the small crystallites formed under the mild conditions employed. SEM inspection of the samples confirmed this suggestion. Uniform in size, 500−1000 nm crystallites are synthesized at 80 °C. The crystallites synthesized at 35 °C are at least 1 order of magnitude smaller. Thus, the sample synthesized for 14 days contains aggregated particles ranging between 30 and 50 nm in size.

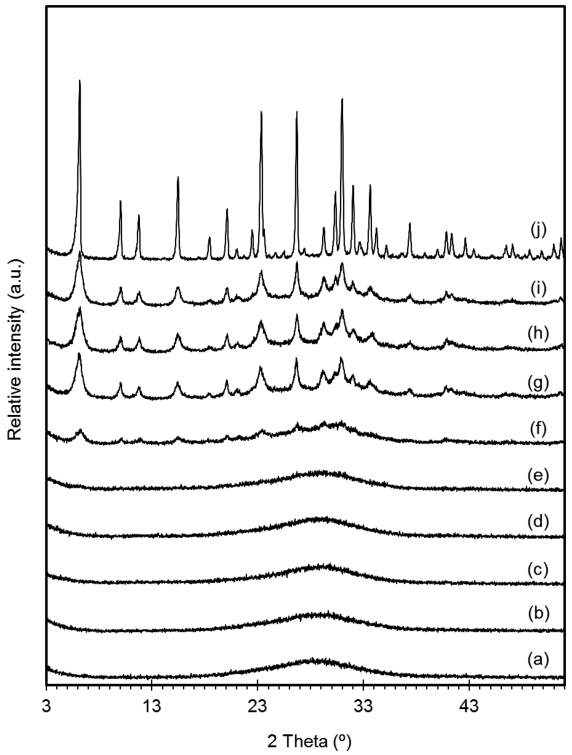

Figure 1. Powder XRD patterns of the solid products obtained after mixing of the initial reactants (a) and after hydrothermal treatment of the gel at 35 °C for 1 (b), 3 (c), 4 (d), 5 (e), 6 (f), 7 (g), 8 (h), and 14 (i) days; (j) shows the XRD pattern of the sample prepared by hydrothermal treatment at 80 °C for 5 days (j).

The TEM images shown in Figure 2 highlight the typical morphological features of the initial amorphous solid and the products obtained after 1, 3, 5, 6, and 7 days of hydrothermal treatment. The solid product recovered immediately after mixing of the initial reactants consists of isometric dense aluminosilicate particles with size of 100−200 nm agglomerated in larger aggregates (Figure 2a). No substantial changes were observed in the size of the particles obtained between 1 and 5 days of hydrothermal treatment (Figure 2b−d). However, with the progression of the crystallization process, the formation of voids in the particles was observed. These voids increased in number and size with the crystallization time. After 5 days of

dx.doi.org/10.1021/cs500153e | ACS Catal. 2014, 4, 2333−2341

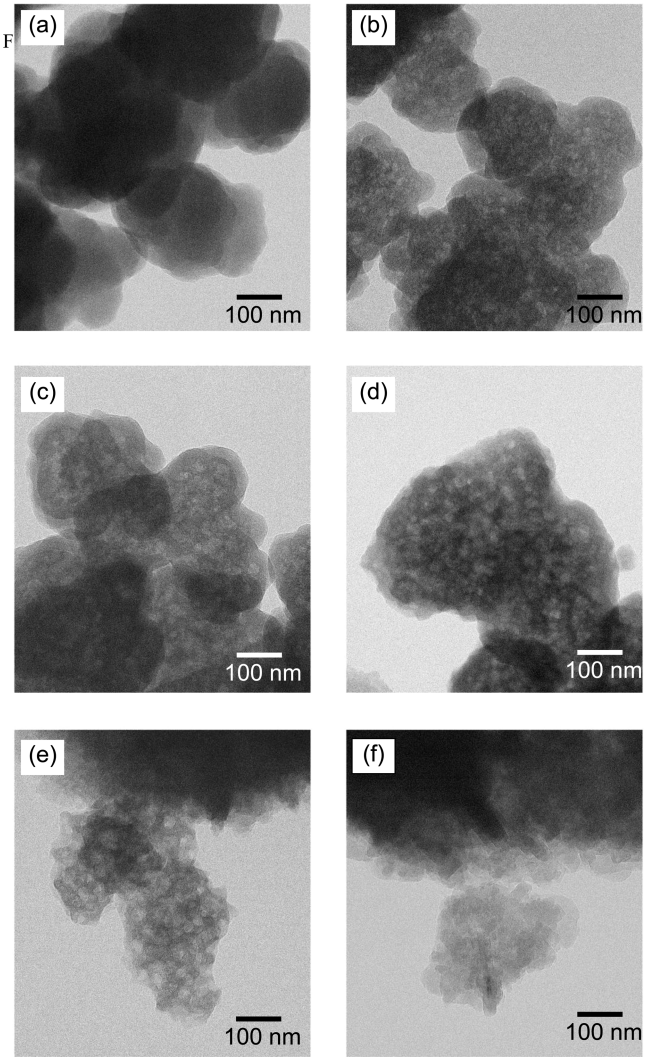

Figure 2. Typical TEM images of recovered solids after mixing the initial reactants (a) and after hydrothermal treatment for 1 (b), 3 (c), 5 (d), 6 (e), and 7 (f) days.

synthesis, the size of the voids was approximately 20−30 nm. These voids were still present in the 6 day sample together with the first zeolite crystallites (Figure 2e). In contrast, the 7 day sample does not contain any voids; only intergrown 10−30 nm in size FAU-type nanoparticles can be observed (Figure 2f). The TEM observation is in good agreement with previous studies,[35,36,55−57] where the presence of voids was proved by a combination of complementary methods including hyperpolarized ^{129}Xe NMR and N_2 sorption measurements and high-resolution TEM.

Surface and textural properties of the series of solids obtained from the initial amorphous solid yielding zeolite X were studied by N_2 adsorption measurements. Nitrogen adsorption−desorption measurements after outgassing at 120, 150, or 250 °C in order to find the most appropriate conditions that do not lead to irreversible changes in the structure of zeolite precursors. As can be seen in Supporting Information (Figure S1A,B) using a lower degassing temperature is more appropriate for amorphous precursors. Higher values for micropore volume and S_{BET} were obtained. Thus, depending on the level of organization, different temperatures were employed in order to study the amorphous aluminosilicate precursors. Representative data for different samples are summarized in Table 1. For instance, the 5 day sample that showed the highest catalytic activity was degassed at 120 °C. Increasing the pretreatment temperature led to a decrease of specific surface area, revealing some irreversible changes in the structure of the catalyst. We relate these changes with noncompleted zeolite elements, whose structure is less robust in respect to a complete crystal. On the other hand, the sample is degassed at temperature that does not allow strongly bound water to be released. Consequently, the N_2 sorption data should be discussed with precaution.

Table 2 summarizes the information on the crystallinity, chemical composition, and catalytic performance of obtained solid products. The amount of recovered solid was also measured and revealed an increase in the product yield with the crystallization time. The physical changes in the gel structure were coupled with changes in the gel chemistry. Thus, the Si/Al molar ratio of the solid changed from 1.6 at the beginning of the process to 1.17 after 7 days of crystallization. The increase of the crystallization time to 14 days resulted in a slight increase of the Si/Al ratio. The global analysis of Na and Al in the solid phase showed Na/Al values in the range of 0.87−1.29, depending on the crystallization stage. In a previous study, we have demonstrated that after mixing the initial reactants, the bulk gel particles comprise mainly silica and alumina, whereas sodium cation is situated in the peripheral part of the particles.[35,36] During the induction period, Na^+ slowly penetrates in the bulk gel, breaking the structure and causing reorganization of the aluminosilicate species. Thermogravimetrical analysis did not reveal a substantial difference between the water content in the amorphous precursor and crystalline product. After 5 days of hydrothermal treatment, the water content in the solid was 22.3 wt %. A slightly higher water release (ca. 24.4 wt %) was observed in the crystalline product taken after 7 days of synthesis (Figure S2). This result suggests

Table 1. Textural Properties of FAU Precursor and FAU Nanocrystals Obtained after Degassing at Different Temperatures

sample						
crystallization time (days)	phase	pretreatment temperature[a] (°C)	BET surface area[b] ($m^2\ g^{-1}$)	external surface area[c] ($m^2\ g^{-1}$)	micropore volume[c] ($cm^3\ g^{-1}$)	mesopore volume ($cm^3\ g^{-1}$)
0	amorphous	120	6.6	3.8	0.002	0.040
		250	42.8	26.5	0.006	0.083
5	amorphous	120	85.3	29.3	0.022	0.089
		150	76.2	30.5	0.018	0.087
		250	38.9	23.5	0.007	0.072

[a]The pretreatment was carried out for 15 h under vacuum at the desired temperature. [b]BET surface area of sample was determined from the nitrogen adsorption−desorption isotherm. [c]Micropore volume was estimated by using the *t*-plot method.

dx.doi.org/10.1021/cs500153e | ACS Catal. 2014, 4, 2333−2341

Table 2. Sample List, Chemical Composition, and Catalytic Performance of Nanosized FAU-Type Crystals and Their Amorphous Precursors

crystallization						
temperature (°C)	time (days)	solid phase	Si/Al (ICP)	Na/Al (ICP)	water content/wt % (TG)	yield in the catalytic reaction[a] (%)
35	0	amorphous	1.54	0.87	20.98	24.5
	1	amorphous	1.68	0.91	n.d.	36.5
	3	amorphous	1.59	0.86	n.d.	43.8
	4	amorphous	1.47	0.92	n.d.	46.2
	5	amorphous	1.36	1.20	22.27	62.8
	6	amorphous + FAU	1.25	1.29	21.39	53.8
	7	FAU	1.17	1.11	24.39	47.0
	8	FAU	1.15	1.27	n.d.	34.7
	14	FAU	1.30	1.10	23.88	29.4
80	5	FAU	1.18	1.00	n.d.	31.4

[a]Reaction conditions: catalyst, 15 mg; temperature, 40 °C; time, 120 min; benzaldehyde, 1.0 mmol (106 mg); ethyl cyanoacetate, 1.0 mmol (113 mg); solvent, EtOH (ca. 3.0 mL).

that the apparently amorphous phase obtained after 5 days of crystallization already had hydrophilicity and water capacity similar to that of the X-ray crystalline product obtained after 7 days.

The short-range order in the series of synthesized samples was studied by solid-state NMR spectroscopy. Figure 3 shows ^{29}Si DD MAS NMR spectra of the initial amorphous solid and products obtained after 5, 6, and 7 days of hydrothermal treatment. The amorphous aluminosilicate formed immediately after mixing of raw materials exhibited a broad peak at about −84.5 ppm. With the extension of the crystallization time, the half width of the peak decreased, and for the 6 days sample, which is a mixture of FAU-type and amorphous material, the resolution of the $(AlO)_4\underline{Si}$ (= $Q^4(4Al)$) peak and the $(AlO)_3\underline{Si}(OSi)$ (= $Q^4(3Al)$) peak became possible. Nanosized FAU-type zeolite obtained after 7 days of crystallization exhibited sharp peaks in the vicinities of −88.5 and −84.5 ppm, which can be assigned to $Q^4(3Al)$ and $Q^4(4Al)$ species, respectively. From these two peak areas, the Si/Al ratio in the framework was calculated to be 1.04 (Figure S3).

Figure 4 depicts the ^{27}Al DE MAS NMR of the initial amorphous solid and samples obtained between 1 and 8 days of hydrothermal treatment. All samples contained tetrahedral Al species, that is, only a peak at about 60 ppm independent of synthesis duration was observed. The initial gel and X-ray amorphous aluminosilicates exhibited a relatively broad peak at 60.5 ppm. This peak became sharper after 6 days of synthesis (Figure 4f) and much more intense after 7 and 8 days of crystallization (Figure 4g,h). For the last three samples, the peak is centered at 63.0 ppm, which is attributed to the changes in the Al−O−Si bond angle.[61] This confirms that the wide bond angle of Al−O−Si in the amorphous product had narrowed (ca. 143.4°), which is defined by a more rigid structure of crystalline FAU-type material.

The short-range order NMR study was complemented by Raman spectroscopic measurements (Figure 5). The series of samples obtained during the induction period (1 to 5 days of crystallization) contained only a broad peak at 502 cm^{-1}, which could be assigned to S4R[42−45] and a shoulder around 570 cm^{-1}. With the increase of the crystallization time the peak at 502 cm^{-1} became narrower and the intensity of shoulder at 570 cm^{-1} decreased. The peaks at 289, 379, and 468 cm^{-1}, attributed to double six rings (D6R), first appeared in the sample treated for 6 days under low temperature hydrothermal conditions. These peaks were much better pronounced in the

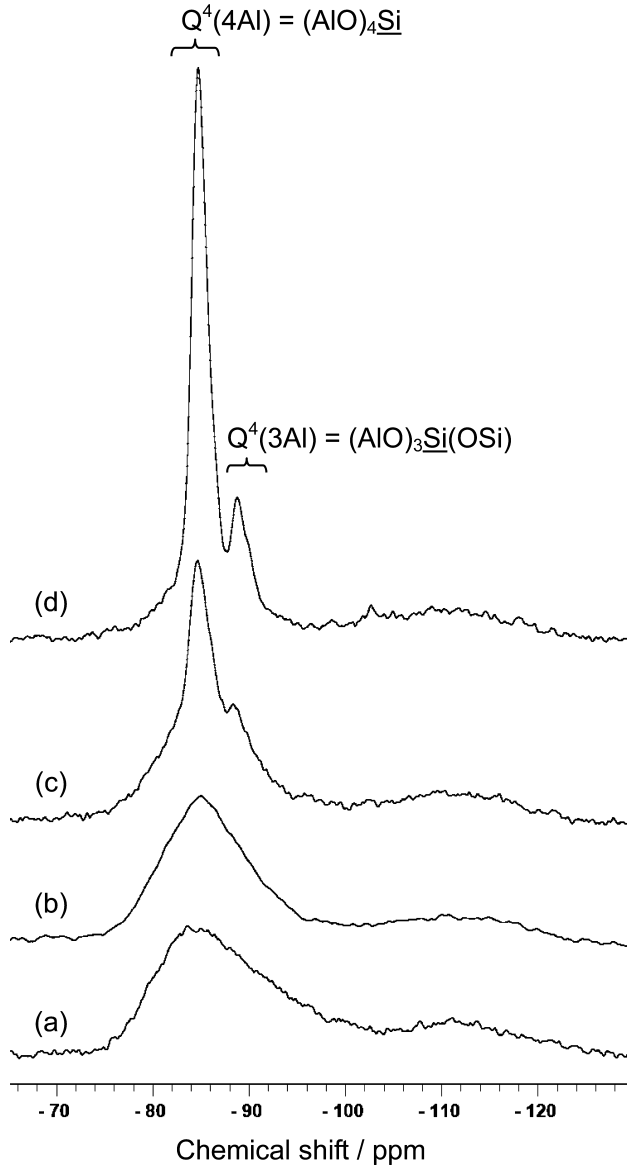

Figure 3. ^{29}Si DD MAS NMR spectra of recovered aluminosilicate solids after 0 h (a) and 5 (b), 6 (c), and 7 (d) days of hydrothermal treatment at 35 °C.

dx.doi.org/10.1021/cs500153e | ACS Catal. 2014, 4, 2333−2341

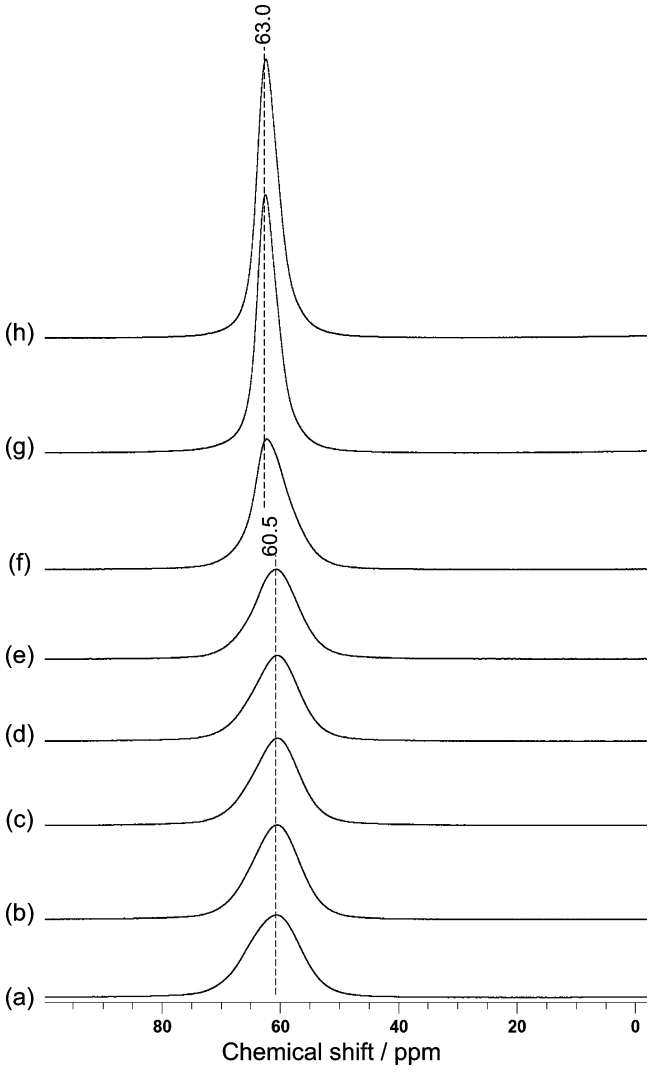

Figure 4. ^{27}Al DE MAS NMR spectra of recovered solids after 0 h (a), 1 day (b) and 3 (c), 4 (d), 5 (e), 6 (f), 7 (g), and 8 days (h) of hydrothermal treatment at 35 °C.

solids obtained after 7 and 8 days of crystallization. Together with the appearance of these peaks the one at 502 cm^{-1} shifted to 510 cm^{-1} and the shoulder at 570 cm^{-1} completely disappeared. The evolution of peak intensity in the system under study was consistent with previous results collected on conventional systems yielding micrometer-sized FAU-type crystals.[42,44,45,47] The analysis of Raman spectra suggested that S4Rs were formed shortly after mixing of the initial reactants. The D6Rs that connect the sodalite cages were detected much latter when the long-range order appeared and the first zeolite crystallites were formed. Thus, the Raman study was in complete agreement with XRD analysis of the samples regarding the evolution of the amorphous to crystalline phase. We should underline, however, that the detection limit of each of the employed physical methods requires at least 3−5 wt % of the solid phase to exhibit a certain level of organization in order to be detected. Therefore, during the induction period and in particular after 5 days of hydrothermal treatment, the presence of semicrystalline units that do not satisfy the condition for X-ray diffraction, but yet possess zeolite organization is more than likely.

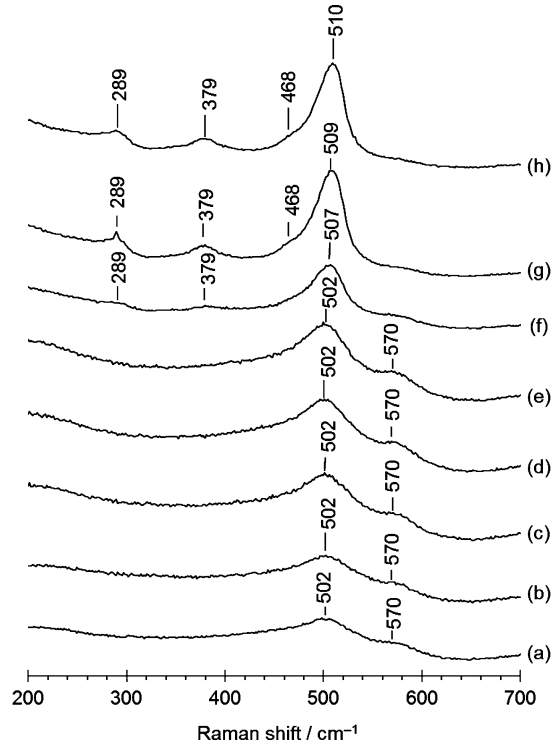

Figure 5. Raman spectra of the solid products obtained after: 0 h (a), 24 h (b) and 3 (c), 4 (d), 5 (e), 6 (f), 7 (g) and 8 days (h) of hydrothermal treatment.

High-energy X-ray diffraction analysis, which provides information on inter atomic distances and thus to the short-range order, has also been used to study the reorganization of the initial gel system. Figure 6 shows the pair distribution function, $G(r)$, of the 0, 5, 6, and 7 day samples. The Q_{max} collected in this study was 25 $Å^{-1}$, and the pair distribution function, $G(r)$, was derived from the Faber−Ziman total structure factor, $S(Q)$. From the $G(r)$ curves, it was possible to identify cation−oxygen, oxygen−oxygen, and cation−cation

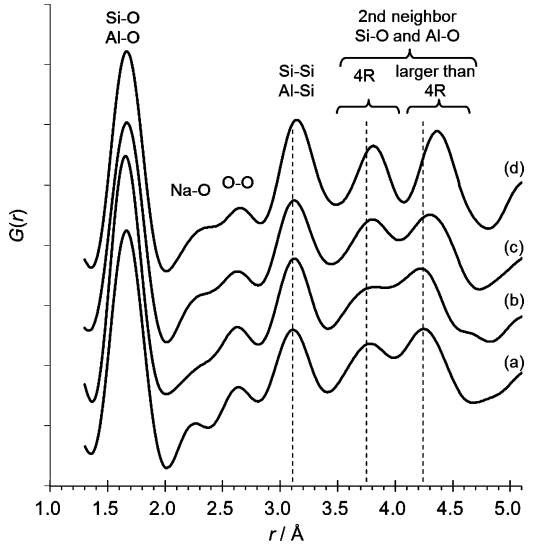

Figure 6. Pair distribution function, $G(r)$, of the initial gel 0 h (a) and recovered samples obtained by hydrothermal treatment at 35 °C for: 5 (b), 6 (c), and 7 (d) days. Note: the data of (b), (c), and (d) were offset vertically at even intervals.

dx.doi.org/10.1021/cs500153e | ACS Catal. 2014, 4, 2333−2341

distances as a function of synthesis time. The first peak in the $G(r)$ is related to Si−O (ca. 1.61 Å) and Al−O (1.71 Å) distances, although the Q range obtained here is insufficient to resolve the two distances (Figure 6). Peaks at 2.2−2.3, 2.6−2.7, and 3.0−3.3 Å are attributed to Na−O, O−O, and T−T (T = Si or Al) distances, respectively. In the $G(r)$ of the 0 h sample (Figure 6a), peaks are centered at 3.7−3.9 and 4.2−4.5 Å, which correspond mainly to the distances from a T atom to the second oxygen (second T−O). The peaks at 3.7−3.9 Å result from the second T−O distances in 4R. Similarly, the peaks at 4.2−4.5 Å result mainly from the second T−O in rings larger than 4R. In the amorphous aluminosilicate formed immediately after mixing raw materials, a large number of 4Rs and larger rings are already present. It should be noted that the distances in the second T−O slightly change during the crystallization, whereas those originating from larger rings (4.2−4.5 Å) shift to a longer distance. This is supported by the fact that T−T (3.0−3.3 Å) also slightly shifts to longer distance with the increase of crystallinity. These results imply that the structure of 4R in amorphous aluminosilicate is similar to that in crystalline FAU-type zeolite as the Raman study indicated. In contrast, the larger rings are more distorted in the initial crystallization stage. They are also less rigid compared to those in the zeolite framework, for instance, 6R in FAU-type structure, as the shorter second T−O (4.2−4.5 Å) distances indicate. Thus, the combined Raman−HEXRD analysis showed that the amorphous aluminosilicate sample comprises rigid four-member rings and randomly distorted larger ring units. The distortion and ordering of ring structures are in good agreement with the peak shift in ^{27}Al MAS NMR. As a consequence of the formation of the crystalline framework that takes place between 5 and 6 days of hydrothermal treatment, the larger rings become more rigid. In this time interval, parts of zeolite structure are present in the solid. These units combine zeolite activity with a structure which is more accessible than FAU-type zeolite.

Catalytic Properties of Amorphous Precursors and Nanosized Zeolite Crystals. The Knoevenagel condensation of benzaldehyde with ethyl cyanoacetate was carried out using the amorphous precursor particles and nanosized FAU-type crystals as a solid base catalyst. Ethyl α-cyanocinnamate was the only product obtained in the catalytic tests (see Scheme 1). The results of catalytic experiments are summarized in Table 2 and Figure 7. The catalytic activity of the series of X-ray amorphous samples increased with the crystallization time. A decrease in catalytic activity was observed with the appearance of a crystalline FAU-type product (6 day sample). On the other hand, the increase of zeolite crystallinity (6−14 days of synthesis) strongly impacted the catalytic performance, and the yield dropped from 62.8% for the 5 day sample to 29.4% for the one obtained after 14 days. This result clearly showed that the catalytic activity of the crystalline product is a function of zeolite crystal size. The extension of the crystallization time led to Ostwald ripening and thus to larger particles which were not appropriate for the reaction under study. This suggestion was confirmed by the catalytic performance of the reference micrometer-sized sample, which showed performance similar to the FAU-type crystals synthesized at 35 °C for 14 days. Thus, solid material obtained after 5 days of hydrothermal treatment showed the highest catalytic activity from all series of amorphous and crystalline samples (Table 2). It is remarkable that an apparently amorphous material exhibited catalytic activity higher than that of nanosized zeolite crystals. This result

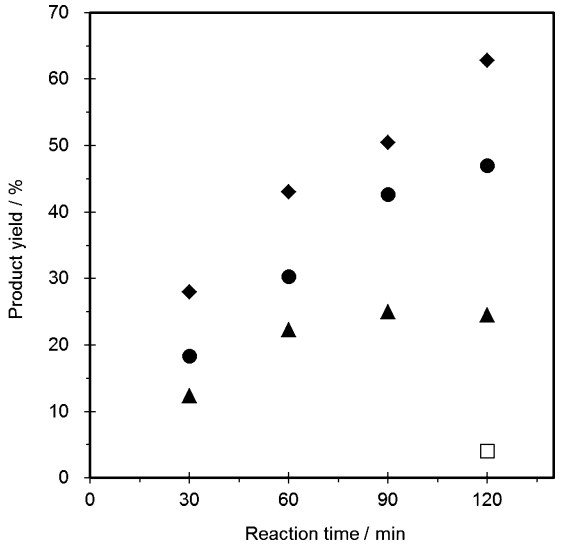

Figure 7. Time course of Knoevenagel condensation of benzaldehyde with ethyl cyanoacetate catalyzed by Na^+-aluminosilicate solids obtained after 0 h (▲), 5 (◆), and 7 days (●) of hydrothermal treatment; the yield of the reaction without using a heterogeneous catalyst (□). Reaction conditions: catalyst, 15 mg; temperature, 40 °C; benzaldehyde, 1.0 mmol; ethyl cyanoacetate, 1.0 mmol; solvent, EtOH (ca. 3.0 mL).

further confirms the conclusion based on the physicochemical characterization of intermediate products of zeolite formation. Namely, prior to the burst of the crystallization process, the solid material already has the composition and the local organization of FAU-type material. The product of the reaction ethyl cyanocinnamate is larger than 12 MR pore openings of FAU-type zeolite. Therefore, in the case of well-formed crystals, the reaction takes place only on the external surface of zeolite particles. Hence, one could anticipate the presence of noncompleted cages in the zeolite precursor that favor the catalytic reaction. Consequently, with the increase of zeolite crystal size, the catalytic activity is expected to decline, which is unambiguously confirmed by the set of catalytic data (Table 2). Therefore, it is not surprising that among the series of FAU-type materials and their intermediates, the best catalytic performance in Knoevenagel condensation is exhibited by a quasi-crystalline material. It is worth recalling that after 5 days of hydrothermal treatment, the solid still contains a system of voids that favor the transport of reactant and products (Figure 2d). At this stage of gel evolution, the formation of colloidal particles that float in the entire reaction volume is observed. These particles are characterized with highly open structure built of semicrystalline zeolite units. It is worth mentioning that the 5 day sample showed a higher product yield compared with that obtained when using a commercial Na−Y (Figure S4).

Table 3 presents the results of the Knoevenagel reaction obtained with the reuse of the 5 day catalyst. In this case, the reaction is performed at higher temperature (70 °C) in order to test the thermal stability of the semicrystalline catalyst and the durability of active sites. The X-ray amorphous catalyst (5 days) shows similar catalytic activity at 40 and 70 °C. This result proves that the catalyst is robust and remains highly efficient at higher temperature. Indirectly, it also provides evidence that the structure of the solid is retained at 70 °C.

Catalytic experiments were complemented with a spectroscopy study in order to evaluate the number of $Na^+\cdots$[Al−O−

dx.doi.org/10.1021/cs500153e | ACS Catal. 2014, 4, 2333−2341

Table 3. Results of Knoevenagel Reaction Catalyzed by a Recycled Zeolitic Precursor (5 Day Sample) at 70 °C

catalyst						
sample	recycle	Si/Al	Na/Al	weight (mg)	reaction time (min)	yield (%)
zeolitic precursor (35 °C, 5 days)	fresh	1.36	1.20	15[b]	60	62.0
				120[c]		61.3
	reuse[a]	n.d.	n.d.	15[b]		61.6

[a]The reuse catalyst was recovered by filtration after the 8-fold scale reaction with a fresh catalyst and the following drying on an oven at 170 °C overnight. [b]Reaction conditions: catalyst, 15 mg; temperature, 70 °C; benzaldehyde, 1.0 mmol (106 mg); ethyl cyanoacetate, 1.0 mmol (113 mg); solvent, EtOH (ca. 3.0 mL). [c]Reaction conditions (8-fold scale of *b*): catalyst, 120 mg; temperature, 70 °C; benzaldehyde, 8.0 mmol (848 mg); ethyl cyanoacetate, 8.0 mmol (904 mg); solvent, EtOH (ca. 24.0 mL).

Si]$^-$ active sites. The interaction of CO_2 with Na^+ was studied by FT-IR spectroscopy. The size of the CO_2 molecule allowed studying both Na atoms situated in the zeolite micropore space and on the external surface. Figure 8 shows the FT-IR spectra

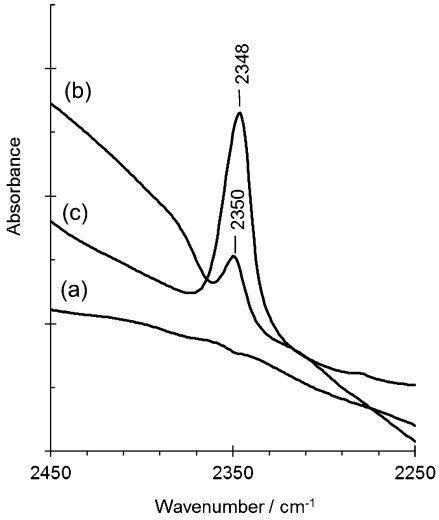

Figure 8. FT-IR observation of the CO_2–Na^+ interaction in Na^+-aluminosilicate solids obtained after 0 h (a) and 5 (b) and 7 days (c) of hydrothermal treatment at 35 °C.

of the initial gel and 5 and 7 day hydrothermally treated samples. The peak characteristic for CO_2 adsorption on sodium atoms is situated at about 2350 cm^{-1}. The intensity of this peak increases with the crystallinity of the samples. The crystalline product (7 days) exhibits a very intense peak at 2348 cm^{-1}; a relatively weak peak can be seen in the spectrum of amorphous (5 days) precursor, and no such peak can be observed in the initial gel. After mixing the initial reactants, there were a few $Na^+\cdots$[Al–O–Si]$^-$ species that can act as active sites. It is also in good agreement with our previous work[35,36] describing concentration of bulk sodium in the peripheral part of the particles. Obviously, a substantial part of polymerized [Al–O–Si]$^-$ species are counterbalanced by protons. Together with the gel reorganization during the induction period, this leads to physical and chemical changes in the gel—the number of active sites increased and reaches a maximum in the fully crystalline zeolite material. However, despite showing the highest amount of basic sites, this material did not show the highest catalytic activity. The most plausible explanation is the diffusion limitations imposed by zeolite channels on the bulky molecule resulting from the Knoevenagel reaction. Thus, the catalyst comprising a lower number but more accessible basic sites showed better performance in ethyl cyanocinnamate synthesis. The latter obviously comprised zeolite structural units with highly accessible semicages that were not limited by 12 MR pore openings. In addition, the short-range zeolite order of these aluminosilicate species provides the necessary strength of the active sites.

CONCLUSIONS

Crystal growth kinetics of zeolite X nanoparticles at 35 °C was studied. First X-ray crystalline material was observed after 6 days of crystallization. Prior to the appearance of a crystalline phase, substantial changes in the ring structure of the aluminosilicate precursor occurred, as revealed by the combined Raman–HEXRD–solid-state NMR analysis. These changes were attributed to the formation of larger structural elements, namely, the sodalite- and supercages of FAU-type structure. Thus, the set of experimental data showed that before the appearance of the crystalline phase, the solid already has some crystalline order. At this stage, the zeolite structure is not completed, which makes this material a very interesting catalyst for reactions involving bulky molecules that cannot be processed with conventional zeolite catalysts.

Knoevenagel condensation was used to test the series of zeolite precursors and nanosized zeolite crystals as base catalysts. The amorphous sodium aluminosilicates obtained for 5 days of hydrothermal treatment exhibited the highest catalytic yield in the reaction of benzaldehyde with ethyl cyanoacetate. This remarkable behavior was attributed to the combination of strong zeolite-type basic sites and the less restricted, more accessible structure of the semicrystalline zeolite units. Thus, the crystal growth kinetics of FAU-type zeolite was used as a tool to control the performance of the catalyst in Knoevenagel condensation.

This approach could be further developed and applied to tune the properties of zeolite-based catalysts that are used in bulky molecules processing.

ASSOCIATED CONTENT

Supporting Information

Further details of nitrogen adsorption–desorption isotherms, TG-DTA, ^{27}Al DE MAS NMR with peak fitting and catalytic data. This material is available free of charge via the Internet at http://pubs.acs.org.

AUTHOR INFORMATION

Corresponding Author

*E-mail: valentin.valtchev@ensicaen.fr.

Notes

The authors declare no competing financial interest.

ACKNOWLEDGMENTS

The authors thank Dr. Shinji Kohara of the Japan Synchrotron Radiation Research Institute (JASRI) for the technical assistance (proposal no. 2012A1278). This paper was financially supported by "Strategic Young Researcher Overseas Visits Program for Accelerating Brain Circulation" from the Japan Society for the Promotion of Science (JSPS) and Yazaki Memorial Foundation of Science and Technology. V.V.

acknowledges the financial support by MicroGreen project (ANR-12-IS08-0001-01).

REFERENCES

(1) Breck, D. W. *Molecular Sieves*; Wiley: New York, 1974.
(2) Schoonheydt, R. A.; Geerlings, P.; Pidko, E. A.; van Santen, R. A. *J. Mater. Chem.* **2012**, *22*, 18705−18717.
(3) Hattori, H. *Appl. Catal., A* **2001**, *222*, 247−259.
(4) Hattori, H. *Chem. Rev.* **1995**, *95*, 537−550.
(5) Davis, R. J. *J. Catal.* **2003**, *216*, 396−405.
(6) Ono, Y. *J. Catal.* **2003**, *216*, 406−415.
(7) Busca, G. *Ind. Eng. Chem. Res.* **2009**, *48*, 6486−6511.
(8) Jones, G. In *Organic Reactions*; Cope, A. C., Ed.; John Wiley & Sons: New York, 1985; Vol. *15*, (Chapter 16).
(9) Richardhein, W.; Melvin, J. *J. Org. Chem.* **1961**, *26*, 4874−4878.
(10) Rand, L.; Haidukewych, D.; Dolinski, R. J. *J. Org. Chem.* **1966**, *31*, 1272−1274.
(11) Moison, H.; Texier-Boullet, F.; Foucaud, A. *Tetrahedron* **1987**, *43*, 537−542.
(12) Muzart, J. *Synthesis* **1982**, 60−61.
(13) Texier-Boullet, F.; Foucaud, A. *Tetrahedron Lett.* **1982**, *23*, 4927−4928.
(14) Corma, A.; Fornés, V.; Martín-Aranda, R. M.; García, H.; Primo, J. *Appl. Catal.* **1990**, *59*, 237−248.
(15) Rodriguez, I.; Cambon, H.; Brunel, D.; Laspéras, M. *J. Mol. Catal. A* **1998**, *130*, 195−202.
(16) Linares, C. F.; Goldwasser, M. R.; Machado, F. J.; Aramis, R.; Rodríguez-Fuentes, G.; Barrault, J. *Microporous Mesoporous Mater.* **2000**, *41*, 69−77.
(17) Goa, Y.; Wu, P.; Tatsumi, T. *J. Catal.* **2004**, *224*, 107−114.
(18) Corma, A.; Fornés, V.; Martín-Aranda, R. M.; Rey, F. *J. Catal.* **1992**, *134*, 58−65.
(19) Angeletti, E.; Canepa, C.; Martinetti, G.; Venturello, P. *J. Chem. Soc., Perkin Trans.* **1989**, *1*, 105−107.
(20) Choudary, B. M.; Kantam, M. L.; Sreekanth, P.; Bandopadhyay, T.; Figueras, F.; Tuel, A. *J. Mol. Catal. A* **1999**, *142*, 361−365.
(21) Subba Rao, Y. V.; Choudary, B. M. *Synth. Commun.* **1991**, *21*, 1163−1166.
(22) Kubota, Y.; Nishizaki, Y.; Ikeya, H.; Saeki, M.; Hida, T.; Kawazu, S.; Yoshida, M.; Fujii, H.; Sugi, Y. *Microporous Mesoporous Mater.* **2004**, *70*, 135−149.
(23) Kubota, Y.; Yamaguchi, H.; Yamada, T.; Inagaki, S.; Sugi, Y.; Tatsumi, T. *Top. Catal.* **2010**, *53*, 492−499.
(24) Hasegawa, T.; Krishnan, C. K.; Ogura, M. *Microporous Mesoporous Mater.* **2010**, *132*, 290−295.
(25) Sugino, K.; Oya, N.; Yoshie, N.; Ogura, M. *J. Am. Chem. Soc.* **2011**, *133*, 20030−20032.
(26) Baerlocher, Ch.; McCusker, L. B.; Olson, D. H. *Atlas of Zeolite Framework Types*, 6th ed.; Elsevier: Amsterdam, 2007. See also: http://www.iza-structure.org/databases/.
(27) Almeida, K. A.; Landers, R.; Cardoso, D. *J. Catal.* **2012**, *294*, 151−160.
(28) Tosheva, L.; Valtchev, V. P. *Chem. Mater.* **2005**, *17*, 2494−2513.
(29) Schoeman, B. J.; Sterte, J.; Otterstedt, J.-E. *Zeolites* **1994**, *14*, 110−116.
(30) Mintova, S.; Olson, N. H.; Bein, T. *Angew. Chem., Int. Ed.* **1999**, *38*, 3201−3204.
(31) Zhu, G.; Qiu, S.; Yu, J.; Sakamoto, Y.; Xiao, F.; Xu, R.; Terasaki, O. *Chem. Mater.* **1998**, *10*, 1483−1486.
(32) Holmberg, B. A.; Wang, H.; Yan, Y. *Microporous Mesoporous Mater.* **2004**, *74*, 189−198.
(33) Li, Q.; Creaser, D.; Sterte, J. *Chem. Mater.* **2002**, *14*, 1319−1324.
(34) Zhan, B.-Z.; White, M. A.; Lumsden, M.; Mueller-Neuhaus, J.; Robertson, K. N.; Cameron, T. S.; Gharghouri, M. *Chem. Mater.* **2002**, *14*, 3636−3642.
(35) Valtchev, V. P.; Bozhilov, K. N. *J. Phys. Chem. B* **2004**, *108*, 15587−15598.
(36) Valtchev, V.; Rigolet, S.; Bozhilov, K. N. *Microporous Mesoporous Mater.* **2007**, *101*, 73−82.
(37) Bo, W.; Hongzhu, M. *Microporous Mesoporous Mater.* **1998**, *25*, 131−136.
(38) Kin, Y.-C.; Jeong, J.-Y.; Hwang, J.-Y.; Kim, S.-D.; Kim, W.-J. *J. Porous Mater.* **2009**, *16*, 299−306.
(39) Ogura, M.; Kawazu, Y.; Takahashi, H.; Okubo, T. *Chem. Mater.* **2003**, *15*, 2661−2667.
(40) Lazarev, A. N. *Vibrational Spectra and Structure of Silicates*; Consultants Bureau: New York, 1972.
(41) Knops-Gerrits, P. P.; de Vos, D. E.; Feijen, E. J. P.; Jacobs, P. A. *Microporous Mater.* **1997**, *8*, 3−17.
(42) Depla, A.; Veyfeyken, A.; Gobechiya, E.; Hartmann, T.; Schaefer, R.; Martens, J. A.; Kirschhock, E. A. *Phys. Chem. Chem. Phys.* **2011**, *13*, 13730−13737.
(43) Dutta, P. K.; Shieh, D. C.; Puri, M. *J. Phys. Chem.* **1987**, *91*, 2332−2336.
(44) Twu, J.; Dutta, K.; Kresge, C. T. *Zeolites* **1991**, *11*, 672−679.
(45) Xiong, G.; Yu, Y.; Feng, Z.-C.; Xin, Q.; Xiao, F.-S.; Li, C. *Microporous Mesoporous Mater.* **2001**, *42*, 317−323.
(46) Yu, Y.; Xiong, G.; Li, C.; Xiao, S. *Microporous Mesoporous Mater.* **2001**, *46*, 23−34.
(47) Fan, F. T.; Feng, Z.-C.; Li, G. N.; Sun, K. J.; Ying, P. F.; Li, C. *Chem.—Eur. J.* **2008**, *14*, 5125−5129.
(48) Greaves, G. N.; Meneau, F.; Sapelkin, A.; Colyer, L. M.; Gwynn, I. A.; Wade, S.; Sankar, G. *Nat. Mater.* **2003**, *2*, 622−629.
(49) Wakihara, T.; Kohara, S.; Sankar, G.; Saito, S.; Sanchez-Sanchez, M.; Overweg, A. R.; Fan, W.; Ogura, M.; Okubo, T. *Phys. Chem. Chem. Phys.* **2006**, *8*, 224−227.
(50) Inagaki, S.; Nakatsuyama, K.; Saka, Y.; Kikuchi, E.; Kohara, S.; Matsukata, M. *Chem. Lett.* **2006**, *35*, 1370−1371.
(51) Inagaki, S.; Nakatsuyama, K.; Saka, Y.; Kikuchi, E.; Kohara, S.; Matsukata, M. *Microporous Mesoporous Mater.* **2007**, *101*, 50−56.
(52) Inagaki, S.; Nakatsuyama, K.; Saka, Y.; Kikuchi, E.; Kohara, S.; Matsukata, M. *J. Phys. Chem. C* **2007**, *111*, 10285−10293.
(53) Sato, K.; Wakihara, T.; Kohara, S.; Ohara, K.; Tatami, J.; Inagaki, S.; Kawamura, I.; Naito, A.; Kubota, Y. *J. Phys. Chem. C* **2012**, *116*, 25293−25299.
(54) Wakihara, T.; Sato, K.; Kohara, S.; Sankar, G.; Tatami, J.; Komeya, K.; Meguro, T.; MacKenzie, K. J. D. *Microporous Mesoporous Mater.* **2010**, *136*, 92−96.
(55) Valtchev, V. P.; Tosheva, L.; Bozhilov, K. N. *Langmuir* **2005**, *21*, 10724−10729.
(56) Valtchev, V. P.; Bozhilov, K. N. *J. Am. Chem. Soc.* **2005**, *127*, 16171−16177.
(57) Itani, L.; Liu, Y.; Zhang, W.; Bozhilov, K. N.; Delmotte, L.; Valtchev, V. *J. Am. Chem. Soc.* **2009**, *131*, 10127−10139.
(58) Ng, E.-P.; Chateigner, D.; Bein, T.; Valtchev, V.; Mintova, S. *Science* **2012**, *335*, 70−73.
(59) Ng, E.-P.; Goupil, J.-M.; Vicente, A.; Fernandez, C.; Retoux, R.; Valtchev, V.; Mintova, S. *Chem. Mater.* **2012**, *24*, 4758−4765.
(60) Faber, T. E.; Ziman, J. M. *Philos. Mag.* **1965**, *11*, 153−173.
(61) Johnson, G. M.; Mead, P. J.; Dann, S. E.; Weller, M. T. *J. Phys. Chem. B* **2000**, *104*, 1454−1463.